

The Correlation between X-ray and UV Properties of BAL QSOs

LuLu Fan,^{1,3} HuiYuan Wang,^{1,2} Tinggui Wang,^{1,2} Junxian Wang,^{1,2} Xiaobo Dong,^{1,2} Kai Zhang,^{1,2} Fuzhen Cheng,^{1,2}

ABSTRACT

We compile a large sample of broad absorption lines (BAL) quasars with X-ray observations from the *XMM-Newton* archive data and Sloan Digital Sky Survey Data Release 5. The sample consists of 41 BAL QSOs. Among 26 BAL quasars detected in X-ray, spectral analysis is possible for twelve objects. X-ray absorption is detected in all of them. Complementary to that of Gallagher et al. (2006) (thereafter G06), our sample spans wide ranges of both BALnicity Index (BI) and maximum outflow velocity (v_{\max}). Combining our sample with G06's, we find very significant correlations between the intrinsic X-ray weakness with both BALnicity Index (BI) and the maximum velocity of absorption trough. We do not confirm the previous claimed correlation between absorption column density and broad absorption line parameters. We tentatively interpret this as that X-ray absorption is necessary to the production of the BAL outflow, but the properties of the outflow are largely determined by intrinsic SED of the quasars.

Subject headings: quasars: absorption lines - X-rays: general

1. INTRODUCTION

About 10%-30% of optically selected QSOs show broad absorption lines (BAL) in their UV spectra, indicative of outflows with velocities up to 0.1c (Hewett & Foltz 2003; Reichard et al. 2003). The similarity in the UV continuum and emission lines between BAL and non-BAL QSOs suggests that BAL QSOs are otherwise normal QSOs viewed in the direction covered by the outflow (e.g. Weymann et al. 1991). One exception to these similarities is that BAL QSOs are soft X-ray faint compared to non-BAL QSOs (e.g. Green et al. 1995; Brinkmann et al. 1999). The weakness in X-rays is interpreted as due to strong absorption

¹Center for Astrophysics, University of Science and Technology of China, Hefei, 230026, China;

²Joint Institute of Galaxies and Cosmology, USTC and SHAO, CAS

³SISSA/ISAS, Via Beirut 2-4, I-34014 Trieste, Italy

rather than intrinsic difference. Evidence for this has been accumulated now from detailed studies of X-ray spectra of a few bright BAL quasars, which display X-ray absorption with column densities from 10^{22} to $\geq 10^{24} \text{ cm}^{-2}$ (Wang et al. 1999; Gallagher et al. 1999, 2002).

Giving the ubiquity of X-ray absorption in BAL quasars, it is natural to ask whether and how the X-ray absorbing gas is connected to the UV BAL phenomenon. It has been known for quite long time that BAL gas should be either confined into small clumps or shielded from the intense soft X-rays in order to match the observed profile. Murray et al. (1995) proposed that the highly ionized gas at the base of disk wind (shielding gas) can naturally filter the soft X-ray radiation to prevent the gas to be over-ionized so that the radiative acceleration is effective (See also Proga et al. 2000). As both UV and X-ray absorbers are part of the continuous outflow, the column densities of the two are expected to be correlated. Indeed, Brandt, Laor & Wills (2000) identified a correlation between the equivalent width of C IV absorption line and the soft X-ray weakness in a sample of bright quasars, including half a dozen BAL QSOs.

Wang et al. (2005, 2007) found that electron scattering of the shielding gas can explain the distribution of continuum polarization in quasars, and the resonant scattering of BAL outflow can explain the observed polarized spectrum of BAL. They further noted that certain special features should appear in the polarized spectrum if the size of the shielding gas is comparable with that of the BAL outflows. As these features are only found in several low-ionization BAL (LoBAL) QSOs (see their paper for details and also Ogle et al. 1999), the shielding gas is likely well inside the BAL outflow except in LoBAL QSOs. A similar conclusion has been reached by studying the X-ray spectra of BAL QSOs (e.g. Gallagher et al. 2004, 2006). On the other hand, as pointed by Wang et al. (2000), in order to keep sufficient opacity in the soft X-ray between $0.2 - 0.3 \text{ keV}$, the absorber must have large column density also of Li-like ions because those ions are responsible for both the soft X-ray absorption between $0.2 - 0.3 \text{ keV}$ and the high ionization UV BALs. Though this band is notoriously difficult to be studied, they argued that at least in three bright low redshift BAL QSOs, the X-ray absorption opacity around $0.2 - 0.3 \text{ keV}$ is large, suggesting very large column density of Li-like ions. However, a relatively small fraction of X-ray absorbing gas at moderate ionization level will be sufficient to suppress the soft X-ray flux.

If the X-ray shielding is critical to the ionization balance in the BAL outflow, which in turn affects the radiative accelerating force on the outflow, one would expect that kinematic properties and column density of BAL outflow will somehow correlate with the properties of the X-ray absorber. In a sample of BAL quasars observed by *Chandra*, G06 found a weak correlation between the maximum outflow velocity (v_{max}) of BAL and the indicator ($\Delta\alpha_{\text{ox}}$) of X-ray absorption. Their finding agrees with the qualitative analysis that the strong soft

X-ray absorption leads to more Li-like ions, thus more efficiently radiative acceleration by UV photons. However just as G06 pointed out that they had only four sources at the low v_{\max} , and their sample of BAL QSOs is biased towards strongly absorbed sources comparing to the BI distribution of SDSS EDR BAL QSOs (Reichard et al. 2003). Giving the importance of this question, more study based on a uniform sample is clearly required.

X-ray absorption is not the only factor that affects the ionization equilibrium of BAL gas. Steffen et al. (2006) showed that the X-ray luminosity of non-BAL QSOs has a large scatter for a given optical luminosity. According to the current popular scenario that BAL and non-BAL are only a matter of whether our line of sight passes through BAL region or not, the intrinsic spectral energy distribution (SED) between UV and X-ray of BAL QSOs should be also diverse. Therefore, it would be interesting to study how the wind properties depend on the intrinsic SED because ionization equilibrium is also closely related to the intrinsic SED. If such a relation does exist, it may offer insight into the driver of the outflows.

In this paper, we present a study of BAL QSOs from SDSS Data Release 5 (DR5) (Adelman-McCarthy et al. 2008) that observed by *XMM-Newton* satellite in X-ray in order to explore the relations between UV and X-ray absorbers as well as the relations between BAL properties and the intrinsic UV to X-ray spectra. In §2 we describe the selection of our C IV BAL QSOs sample and the data analysis in §3. We show our results and discuss the underlying physics in §4. Finally, we summarize our results in §5. Throughout the paper, we assume the cosmological parameters $H_0 = 70 \text{ km s}^{-1} \text{ Mpc}^{-1}$, $\Omega_M = 0.3$ and $\Omega_\Lambda = 0.7$.

2. THE BAL QUASARS OBSERVED BY *XMM-Newton*

Starting from the spectroscopic quasar sample in the SDSS DR5 (Adelman-McCarthy et al. 2008), we compiled a sample of definitive C IV BAL quasars that have been observed by *XMM-Newton* either serendipitously or as a target. We restricted the redshift $1.5 < z < 4.0$ in order to make sure that the C IV $\lambda 1549$ is shifted into the SDSS wavelength regime (3800–9200Å). We matched these quasars with *XMM-Newton* pointing, and resulted in 225 quasars in the FOV of *XMM-Newton* observation to date of April,2007.

We measured the BALnicity Index (BI, Weymann et al. 1991) and the maximum outflow velocity for these 225 quasars using our own fitting code (see §3.2 for detail). We adopted the conventional definition for the BAL QSO: the equivalent width (in km s^{-1}) of any contiguous absorption (at least 10% below the continuum) exceeds 2000 km s^{-1} that falls between $3000\text{--}25000 \text{ km s}^{-1}$ blueshifted from the systematic redshift (Weymann et al. 1991). All quasars with non-zero BI were checked by eye, and ambiguous sources were removed.

Our final sample consists of 41 C IV BAL quasars, including 5 LoBAL quasars, 22 HiBAL quasars, and 14 BAL quasars with unknown BAL subtype because Mg II is not within the SDSS spectral coverage. Most (25) of them have been included in the large BAL QSOs catalog from SDSS DR3 (Trump et al. 2006). In comparison with G06, BAL quasars in our sample cover somewhat larger ranges of redshift ($1.579 - 3.776$) and UV luminosity ($\log(l_{2500}): 30.212 - 32.230$), and are fainter on average (31.055). Our sample has more uniform distributions in BI ($3 - 4610 \text{ km s}^{-1}$ with an average 1101 km s^{-1}) and in v_{max} ($5306 - 25000 \text{ km s}^{-1}$ with an average 14482 km s^{-1}) while G06's sample consists mainly of BAL QSOs with the large BI (with an average 3437 km s^{-1}).

We notice that there are only four *XMM-Newton* targeted objects: SDSS J091127.61+055054.1, SDSS J111816.95+074558.1, SDSS J152553.89+513649.1 and SDSS J154359.44+535903.2 (Table 1). The first two are the lensed BAL QSOs (Bade et al. 1997), which will be excluded from the following correlation analysis. The third quasar was observed because of its high optical polarization (Shemmer et al. 2005). The fourth object was observed because of its X-ray detection by previous missions, thus may bias towards X-ray bright sources (Grupe et al. 2003).

Some radio loud BAL QSOs show anomalous X-ray properties in comparison with radio quiet counterparts (Brotherton et al. 2006; Wang et al. 2008). In order to mark such sources, we calculate the radio-to-optical flux ratios, $R_i = \log(S_{1.4\text{GHz}}/S_i)$, following the definition of Ivezić et al. (2002). The flux densities at 1.4 GHz, $S_{1.4\text{GHz}}$, are taken from the Faint Images of the Radio Sky at Twenty centimeters survey (FIRST; White et al. 1997). We estimate the R_i upper limits by taking the 2σ errors as the upper limit of radio flux density. Only, three sources (SDSS J092345.19+512710.0, SDSS J133004.72+472301.0 and SDSS J133553.61+514744.1) have radio counterparts with the measured flux density of 1.72 mJy, 1.18 mJy and 2.92 mJy, which give $R_i=1.42$, 1.18 and 1.14, respectively.

We listed our sample in Table 1 including the SDSS ID, the redshift, i band fiber magnitude of SDSS, the flux density at rest-frame 2500\AA (f_{2500}), Galactic N_{H} from Dickey & Lockman (1990), the BAL subtype and the radio-to-optical flux ratios R_i . Also we listed the BI and v_{max} in Table 1 (see §3.2). The values of f_{2500} are calculated either by averaging the flux densities in the rest-frame range of $2500 \pm 20\text{\AA}$ or by extrapolating from the continuum given by our fitting code.

3. DATA ANALYSIS

3.1. X-ray Data Analysis

The X-ray data were retrieved from *XMM-Newton* Science Archive (XSA) and prepared using *SAS* 7.0.0 with the most recent calibration files. We extracted the background lightcurve above 10 keV, and the light curve was used to filter the data obtained during the flaring background periods using a threshold of 1.0 count s⁻¹ for PN and 0.5 count s⁻¹ for MOS. A sliding box cell detection algorithm (*eboxdetect*) was applied to the images obtained by PN-CCD detector and two MOS-CCD detectors in the soft (0.3 – 2.0 keV), hard (2.0 – 10.0 keV) and full (0.3 – 10.0 keV) bands to search for X-ray sources. We selected $L = -\ln(P) = 10$ as the minimum detection likelihood value, which in turn corresponded to a probability of Poissonian random fluctuations of the counts of $P = 4.5 \times 10^{-5}$. Among 41 BAL quasars, 26 were detected in the full band and 25 (13) were detected in the soft (hard) bands at least on one EPIC instrument. The spectra were accumulated from a circle region with a 30' radius except for two sources locating close to the edge of the CCD whereas a circle with 20' radius was adopted. The backgrounds were extracted from a source-free annulus surrounding each target on the two MOS-CCD detectors and from a source-free circle along the read-out direction on the pn-CCD detector. The photon counts were extracted from the circular source regions centered on the SDSS optical positions with the mentioned radius and the aperture corrections were performed (See Table 2). For non-detections the upper limits of counts are the 90% confidence limits from Bayesian statistics (Kraft et al. 1991). The redistribution matrix file (*rmf*) and auxiliary response file (*arf*) were generated using the tasks *rmfgen* and *arfgen* respectively.

X-ray spectral modelling are performed using the package *XSPEC* (Arnaud 1996). We fit all the spectra with a uniform model, an absorbed power law. It is found that the photon index Γ of the power-law is around 2.0 with a small scatter for radio-quiet quasars (George et al. 2000; Reeves & Turner 2000). The broad band X-ray spectra of BAL QSOs are quite similar to those of radio quiet non-BAL QSOs, (Gallagher et al. 2002; Chartas et al. 2002, 2003; Aldcroft & Green 2003; Grupe et al. 2003; Page et al. 2005), therefore, in following analysis, Γ is fixed to 2.0. Both the Galactic neutral HI absorption and an intrinsic absorption are included in the model. The Galactic neutral HI column density is fixed at the value derived from Galactic HI maps (Dickey & Lockman 1990) (See Table 1). Due to limited count rates and the large uncertainties, we do not consider more complex X-ray absorption models (e.g., a partially covering or ionized absorber), and just adopt a simple neutral absorption with a solar chemical composition at the source rest frame (*zwabs* in *XSPEC*) (Morrison & McCammon 1983) for the intrinsic absorption.

To deal with very different X-ray counts available, two different methods are used to estimate the intrinsic absorption column density. The X-ray spectrum is fitted directly with an absorbed power-law if the source is detected in the both soft and hard band. Only the intrinsic absorption and the power-law normalization are free parameters. Other parameters, including redshift, the Galactic neutral absorption and the photon index Γ , are fixed to the proper values. Either χ^2 -statistic or C-statistic (Cash 1979) is taken as the merit of the fit depending on the net source counts. If the net source counts are greater than 100, the spectrum is re-binned with at least 15 counts per bin, and the fit is performed by minimizing χ^2 . Otherwise, the spectrum is not binned and the fit is performed by minimizing the C-statistics. In order to test the validity of the fixed Γ power-law model, we make Γ free to fit eight sources with greater than 100 counts. The average value of Γ of six sources is about 1.90, which is very close to 2.0. The other two (SDSS J091127.61+055054.1 and SDSS J100728.69+534326.7) show a rather flat spectra with $\Gamma \sim 1.2$. Page et al. (2005) mentioned that SDSS J091127.61+055054.1 should be better modelled by a broken power law with the values of Γ 0.92 and 1.96, respectively. The fitted intrinsic absorptions are very similar to those listed in Table 3 except the two flat spectral sources. A flat spectrum can be caused by complex absorption, strong reflection component or an intrinsic flat power-law. Because all other six sources show normal X-ray spectra and there is no evidence for strong Fe $K\alpha$ in the X-ray spectrum, we believe that the flat spectra in these two objects are caused by complex absorptions. However, due to limit counts available, we will not try more complicated models.

For those sources detected only in hard or soft band, the upper/lower limit of the column density of intrinsic absorption is estimated from the hardness ratios, defined as $HR = (h-s)/(h+s)$, where h and s are referred to the hard and soft band counts, respectively. First for each source, we calculate hardness ratios for a grid absorbed power-law models with column densities in the range of $10^{20} - 10^{24} \text{ cm}^{-2}$ using the *arf* and *rmf* at the source position. The observed hardness ratio is then compared to the models and then the upper/lower limit of the intrinsic absorption could be derived.

In order to compare our sample with that of G06, we also calculate α_{ox} , $\Delta\alpha_{\text{ox}}$ and $\alpha_{\text{ox}}(\text{corr})$, $\Delta\alpha_{\text{ox}}(\text{corr})$, defined in the G06¹, as follows. First, the above hardness ratios for all BAL QSOs in the sample were estimated. Hardness ratios for a grid of power-law models only absorbed by the Galactic column density in that direction were then calculated using the *XSPEC*. The observed HR was compared to the model HRs to estimate the photon index Γ_{HR} . With the best fitted photon-index, the normalization at 1 keV was derived from the count-rates. The Galactic absorption corrected 2 keV flux is determined from the

¹Our definition of the soft (s : 0.3 – 2.0 keV) and hard (h : 2.0 – 10.0 keV) bands is slightly different from theirs (s : 0.5 – 2.0 keV; h : 2.0 – 8.0 keV).

model. We defined the UV to X-ray broad band spectral index as $\alpha_{\text{ox}} = 0.384 \log(f_{2\text{keV}}/f_{2500})$ (Tananbaum et al. 1979). It is found that α_{ox} is correlated with the optical luminosity of quasars (Yuan et al. 1998; Avni & Tananbaum 1986; Wilkes et al. 1994; Green et al. 1995), though its reality has been questioned by Yuan et al. (1998); Tang et al. (2007). Following G06, we introduce a quantity of $\Delta\alpha_{\text{ox}} = \alpha_{\text{ox}} - \alpha_{\text{ox}}(l_{2500})$ to characterize the weakness of the X-ray emission of the quasar relative to the average quasars at that UV luminosity, where $\alpha_{\text{ox}}(l_{2500})$ was the expected α_{ox} based on the 2500 Å monochromatic luminosity, l_{2500} (Strateva et al. 2005). For sources not detected in both band, an upper limit to the X-ray flux was derived by assuming $\Gamma = 1.0$. Finally, $\alpha_{\text{ox}}(\text{corr})$ and $\Delta\alpha_{\text{ox}}(\text{corr})$ were calculated from an “absorption-corrected” value for the 2 keV flux density estimated by a fixed $\Gamma = 2.0$ power-law model normalized by the counts rate in the observed-frame 2-10 keV bandpass. Note that for two lensed sources, SDSS J091127.61+055054.1 and SDSS J111816.95+074558.1, we do not calculate $\Delta\alpha_{\text{ox}}$ or $\Delta\alpha_{\text{ox}}(\text{corr})$ since their intrinsic l_{2500} are unknown.

3.2. Ultraviolet Spectral Analysis And C IV Absorption-Line Parameters

Following the procedures described in Zhou et al. (2006), we calculate both the BI of C IV and Mg II absorption lines and their maximum outflow velocity, v_{max} . Briefly, we use the SDSS composite quasar spectrum Vanden Berk et al. (2001) as the template for continuum and emission line spectrum. The template is reddened and scaled to match the observed quasar spectrum in the absorption line free windows. The BI of C IV and Mg II are calculated following the definition given by Weymann et al. (1991) and Reichard et al. (2003), respectively, as follows,

$$BI = \int_{0 \text{ or } 3000}^{25000} dv \left[1 - \frac{F^{\text{obs}}(v)}{0.9F^{\text{fit}}(v)} \right] C(v) \quad (1)$$

where $F^{\text{obs}}(v)$ and $F^{\text{fit}}(v)$ are the observed and fitted fluxes, respectively, as a function of velocity in km s^{-1} from the systematic redshift within the range of each absorption trough and

$$C(v) = \begin{cases} 1.0, & \text{if } \left[1 - \frac{F^{\text{obs}}(v)}{0.9F^{\text{fit}}(v)} \right] > 0 \text{ over a continuous interval of } \gtrsim W \text{ km s}^{-1} \\ 0, & \text{otherwise} \end{cases} \quad (2)$$

The integral in equation (1) starts from $v = 3000 \text{ km s}^{-1}$ for C IV and from $v = 0 \text{ km s}^{-1}$ for Mg II. The threshold interval in equation (2) is $W = 2000 \text{ km s}^{-1}$ for C IV and from $W = 1000 \text{ km s}^{-1}$ for Mg II. Five sources show the non-zero BI of Mg II consistent with $\sim 10\%$ fraction of low ionization BAL QSOs. The maximum outflow velocity are calculated, simultaneously. The BI and v_{max} of C IV absorption lines are listed in Table 1.

Finally, we also remeasure the BI and v_{\max} for G06’s sample on the LBQS spectra (Foltz et al. 1987, 1989; Hewett et al. 1991; Chaffee et al. 1991; Morris et al. 1991; Hewett et al. 1995) using our method because we will combine G06’s sample with ours in the statistical analysis between the properties of X-ray and UV. We find that our measurements of either BI or v_{\max} are well correlated with those of G06 although there is considerable scatter. For six objects both in this sample, the SDSS BAL QSO sample of Trump et al. (2006) and in G06, our measurements appear in between theirs. Note that the results of correlation analysis by using G06’s BI and v_{\max} are very similar to those obtained by using ours.

4. RESULTS AND DISCUSSION

4.1. X-ray Properties Of BAL QSOs

To investigate the general X-ray properties of our SDSS/*XMM-Newton* BAL sample (this paper), we try to measure the intrinsic absorption adopting a simple neutral absorption. However, only 12 of 41 sources can be fitted directly to give the intrinsic absorption column densities N_{H} in the range $\sim 4 \times 10^{21}$ to $\sim 2 \times 10^{23} \text{ cm}^{-2}$. For 14 sources, upper/lower limits can be placed by the hardness ratios HR. The final sample spans a wide range of intrinsic absorption column densities from $< 10^{20} \text{ cm}^{-2}$ to $\sim 10^{24} \text{ cm}^{-2}$ (Table 3). The lowest limit is obtained for the LoBAL QSO, SDSS J092238.43+512121.2. We have rechecked the optical spectrum, the identification of this quasar as LoBAL might be questionable because of the presence of narrow absorption lines. Notably, five LoBAL QSOs do not show stronger absorption than HiBAL QSOs.

Following G06, we measure α_{ox} or place upper/lower limits on it, which ranges from -1.36 to -2.26 with an average -1.86 (Table 3). Similar to G06, we show the $\Delta\alpha_{\text{ox}}$, to account for the luminosity dependence of α_{ox} (Table 3, see also the dot-dashed line in Fig. 1). The average value of $\Delta\alpha_{\text{ox}}$ is -0.25 , suggesting that 2 keV X-ray luminosities (at rest frame) of our SDSS/*XMM-Newton* BAL sample are roughly three times fainter than the SDSS/*ROSAT* non-BAL sample (Strateva et al. 2005). And in Table 3 we also present the $\alpha_{\text{ox}}(\text{corr})$ and $\Delta\alpha_{\text{ox}}(\text{corr})$ as a surrogate of the intrinsic X-ray properties of BAL QSOs. $\alpha_{\text{ox}}(\text{corr})$ is calculated by assuming $\Gamma = 2.0$ and using the hard-band counts rate to normalize the X-ray continuum and $\Delta\alpha_{\text{ox}}(\text{corr}) = \alpha_{\text{ox}}(\text{corr}) - \alpha_{\text{ox}}(l_{2500})$ (see G06 or §3.1 for the definition). We find $\Delta\alpha_{\text{ox}}(\text{corr})$ in the range from -0.36 to 0.29 with an average value of 0.11 , which indicates our SDSS/*XMM-Newton* BAL sample is slightly X-ray brighter, relative to the average quasars at that UV luminosity, than the SDSS/*ROSAT* non-BAL sample (Strateva et al. 2005, see Fig. 1). The X-ray brighter of our sample may be due to the relative shallower detection threshold of *XMM-Newton* relative to *Chandra*. Comparing the

$\Delta\alpha_{\text{ox}}(\text{corr})$ distribution of the LBQS/*Chandra* BAL sample(G06) with the SDSS/*ROSAT* non-BAL sample(Strateva et al. 2005, figure 2 of G06) one can find the LBQS/*Chandra* BAL sample(G06) is slightly intrinsic X-ray weaker with a median $\Delta\alpha_{\text{ox}}(\text{corr}) = -0.14$ than the normal QSOs. Alternately, even hard X-rays are absorbed in the LBQS/*Chandra* BAL sample(G06) so that the simple assumption is broken down (See G06 or §3.1 for detail). We have carried out simulations to test this effect. Using *XSPEC*, we simulate the dependence of the $\Delta\alpha_{\text{ox}}(\text{corr})$ on the varying neutral hydrogen column density N_{H} . We assume that $\Delta\alpha_{\text{ox}}(\text{corr})$ equals to zero for a single $\Gamma = 2$ power-law with $N_{\text{H}} = 10^{20} \text{ cm}^{-2}$ at the redshift 2. We find that an absorption column density of $3 \times 10^{23} \text{ cm}^{-2}$ is required in order to account for the mean offset, about -0.14 , of $\Delta\alpha_{\text{ox}}(\text{corr})$ of the LBQS/*Chandra* BAL sample(G06) relative to the SDSS/*ROSAT* non-BAL sample(Strateva et al. 2005). If this is the main cause, most of X-ray weak sources in the LBQS/*Chandra* BAL sample(G06) will have a column density at least order of this. Future X-ray observation is certainly needed to assess this.

Either intrinsic X-ray weak or large column density of absorber may indicate that the LBQS/*Chandra* BAL sample(G06) is biased in X-ray properties. Their sample obviously has larger values of BI and v_{max} than the SDSS BAL QSOs(Reichard et al. 2003) and is not uniform on UV properties too. Note that our SDSS/*XMM-Newton* BAL sample is more uniform, especially on UV properties, and can be used as a complement to the LBQS/*Chandra* BAL sample(G06). For direct comparison, we show the distribution of $\Delta\alpha_{\text{ox}}$ for the SDSS/*ROSAT* non-BAL sample(Strateva et al. 2005) and $\Delta\alpha_{\text{ox}}(\text{corr})$ for our SDSS/*XMM-Newton* BAL sample(this paper) and the LBQS/*Chandra* BAL QSO sample(G06) in Fig. 1. In the following we used the combined sample of ours 41 and G06's 35 sources to study the relations between X-ray and UV properties. Note again, the UV properties of the LBQS/*Chandra* BAL QSO sample(G06) used in this paper are obtained by using our procedures so that we can use the consistent definition of BI and v_{max} . We also use the hardness ratios presented in G06 to calculate N_{H} of these G06 QSOs following the same approach as we have done for *XMM-Newton* sources.

4.2. X-ray And UV Absorptions

One of the purposes of this paper is to study the relationship between the UV and X-ray absorbers. It is generally believed that the X-ray absorber shields the disk winds from soft X-rays and makes line driving more efficient. A naive deduction is that the properties of UV and X-ray absorptions are correlated. Basing on this idea, G06 presented a correlation analysis between the X-ray absorption using $\Delta\alpha_{\text{ox}}$ as an indicator and the UV absorption

properties such as BI, DI, v_{\max} and f_{deep} . They found only a weak correlation between $\Delta\alpha_{\text{ox}}$ and v_{\max} . We will carry out a similar analysis using a larger sample covering more uniformly the whole BI range. In the following analysis, we will use Kendall- τ test to quantify the significance of a correlation.

First, we check whether $\Delta\alpha_{\text{ox}}$ is a good indicator of X-ray absorption. In the left panel of the Fig. 2, we show N_{H} versus $\Delta\alpha_{\text{ox}}$ for the combined subsample of 51 BAL QSOs that N_{H} is obtained either from spectral fit or from HR analysis. Similar to G06, we find a clear correlation between the two quantities. The probability for null hypothesis is less than 0.01% using non-parametric Kendall τ -test (See Table 4). Then we compare the redshift distributions of sources with $\Delta\alpha_{\text{ox}} > -0.2$ and $\Delta\alpha_{\text{ox}} < -0.2$. The result is their distributions are very similar, which indicates that the correlation between N_{H} and $\Delta\alpha_{\text{ox}}$ is not from selection effect of redshift. These suggest that $\Delta\alpha_{\text{ox}}$ can be used as a measure for X-ray absorption indeed.

Next, we examine the correlations between BAL properties and the X-ray absorption column density N_{H} (Fig. 4) measured through X-ray spectral fit or HR analysis. We do not find any correlation with a probability of null hypothesis less than 1% (Table 4). However, a weak correlation between BI and N_{H} cannot be rejected because the large uncertainty in the N_{H} measurement may reduce the significance of a weak correlation to the measured level (2%).

We show $\Delta\alpha_{\text{ox}}$ versus BI and $\Delta\alpha_{\text{ox}}$ versus v_{\max} in Fig. 3. Two lensed BAL QSOs are excluded from following analysis because their UV and X-ray light may have been differently amplified. There appears a correlation between $\Delta\alpha_{\text{ox}}$ and BI with the probability for null hypothesis of only 0.05% (Table 4). The correlation appears not linear, rather there is an upper envelope. Since LoBAL QSOs may be different from the HiBAL QSOs (Boroson & Meyers 1992; Wang et al. 2007), we also make Kendall test for 45 HiBAL QSOs only. The correlation is marginally significant with a null probability of 1%. The decrease in significance is caused by reducing the sample size. However, we do not find any significant correlation between v_{\max} and $\Delta\alpha_{\text{ox}}$, which was seen in G06, in neither the whole sample nor in the HiBAL subsample with a null probability of 5% and 68%, respectively (Table 4). Comparison with the LBQS/*Chandra* BAL sample (G06), our sample has a handful BAL QSOs on the upper right of the figure. These BAL QSOs destroy the weak correlation trend of v_{\max} vs $\Delta\alpha_{\text{ox}}$ in the LBQS/*Chandra* BAL sample (G06). These correlations are more or less similar to the correlations using N_{H} with an exception of higher significance. It is worthwhile to note that $\Delta\alpha_{\text{ox}}$ reflects a combination of the X-ray absorption and the intrinsic deviation to the average quasar SED. Therefore, one must be careful as using it as an indicator of X-ray absorption. We will discuss below the implication of these results.

4.3. Intrinsic X-ray Properties And The Outflow

Previous studies have shown that UV properties, such as the blueshift and the equivalent width of C IV emission line, are correlated with X-ray to optical flux ratio for non-BAL QSOs (e.g. Baskin & Laor (2004); Richards (2006)). It would be interesting to explore whether the BAL properties are correlated with the intrinsic α_{ox} . Unlike the correlation with X-ray absorption, such correlation should give information for the primary driver of the outflow. Here we use a corrected α_{ox} i.e. $\alpha_{\text{ox}}(\text{corr})$ to represent the intrinsic α_{ox} and investigate its relation with the UV absorption line properties. We also study the correlations between UV properties and $\Delta\alpha_{\text{ox}}(\text{corr})$ so that we can compare the results with those in previous section and G06. We note that the range of UV luminosity, l_{2500} , for the combined sample is only 2 dex, which introduce a scatter in $\alpha_{\text{ox}}(\text{corr})$ through $\alpha_{\text{ox}} \sim l_{2500}$ correlation, of less than 0.27, a factor of about 2.5 smaller than the dynamic range of $\alpha_{\text{ox}}(\text{corr})$. Therefore, the difference between $\Delta\alpha_{\text{ox}}(\text{corr})$ and $\alpha_{\text{ox}}(\text{corr})$ should be small in correlation analysis. This is verified below that the relationships between $\Delta\alpha_{\text{ox}}(\text{corr})$ and UV properties have a very similar behavior as those between $\alpha_{\text{ox}}(\text{corr})$ and UV properties.

Before exploring UV and X-ray connection, we first check whether $\alpha_{\text{ox}}(\text{corr})$ and $\Delta\alpha_{\text{ox}}(\text{corr})$ are affected by the X-ray absorption or not. We plot N_{H} versus $\Delta\alpha_{\text{ox}}(\text{corr})$ on the right panel of Fig. 2. There is no apparent correlation between the two quantities. Kendall test gives a probability of chance coincidence of 36% (Table 4). Therefore, we can conclude that there is no evidence that $\alpha_{\text{ox}}(\text{corr})$ and $\Delta\alpha_{\text{ox}}(\text{corr})$ are significantly affected by X-ray absorption.

We then explore the correlations between $\alpha_{\text{ox}}(\text{corr})$ and BI or v_{max} with Kendall and Spearman tests. We find that $\alpha_{\text{ox}}(\text{corr})$ is significantly correlated with both BI and v_{max} with a Null probability of less than 0.1% for either test (See Fig 5; also Table 4). The correlation is still very significant ($P < 0.1\%$) for HiBAL QSO subsample (45 QSOs). For clarity we show only QSOs detected in the hard X-ray band in Fig.6. Furthermore, these QSOs are more important for the Kendall and Spearman tests than the rest objects, and can give us a clear trend about these correlations. We note that one LoBAL QSOs, SDSS J133553.61+514744.1, which appears largely discrepant with the main sample in Fig. 5 and 6. This quasar has very steep X-ray photon index $\Gamma \sim 2.56$ so that our ‘absorption-correction’ underestimate the intrinsic X-ray luminosity. If we set $\alpha_{\text{ox}} = -1.82$ as the lower limit of $\alpha_{\text{ox}}(\text{corr})$ (it is reasonable since $\alpha_{\text{ox}}(\text{corr})$ is larger than α_{ox}), this quasar would move rightward and is consistent with other quasars. The correlations between $\Delta\alpha_{\text{ox}}(\text{corr})$ and UV properties are very similar to above correlations using $\alpha_{\text{ox}}(\text{corr})$ except the latter appear slightly more significant (Table 4). This may indicate that the dependence of UV properties on $\alpha_{\text{ox}}(\text{corr})$ is more fundamental than on $\Delta\alpha_{\text{ox}}(\text{corr})$.

Is it possible that these correlations are introduced by some selection effect in the sam-

ple? If it is the case this effect would tend to miss the objects which occupy the bottom-left (X-ray weak and high UV absorption) and top-right (X-ray strong and low UV absorption) corners of Fig. 5 and 6. Note that the sample selections of ours and G06’s are both based on the optical luminosity and have nothing to do with the X-ray properties. If the relative X-ray luminosity is uncorrelated with BAL properties it is hard to understand why G06 and we select the objects at the bottom-right(top-left) corner but miss those at the bottom-left(top-right) corner. Since objects at top-right (bottom-left) corners, if they really exist, should have the same optical properties as these at top-left (bottom-right). All of these analysis indicate the correlations between the intrinsic α_{ox} and the properties of UV absorber are real. We discuss the implications of the correlations in details in the next subsection.

4.4. Discussion

Using a larger and more uniform sample, we reexamine the correlations between BAL properties and X-ray absorption presented in G06. Two indicators of X-ray absorption, N_{H} and $\Delta\alpha_{\text{ox}}$, are used in the work. We identify the correlation between $\Delta\alpha_{\text{ox}}$ and BI as the only significant one. In particular, we do not find the correlation between $\Delta\alpha_{\text{ox}}$ and v_{max} claimed in G06, and any correlation between N_{H} and the UV absorption properties. Although we can not rule out a weak correlation between N_{H} and the UV absorption line properties due to relative large error bar of N_{H} our results clearly suggest that X-ray absorption is *not* the major factor that determines UV absorption properties. Given the fact that almost all BAL QSOs show strong absorption in X-ray, it seems that X-ray absorption is a necessary condition for launching of the BAL winds, but the properties of the wind depend on other factors. As shown above, the observed correlation between $\Delta\alpha_{\text{ox}}$ and BI may be the secondary effect of the correlation between BI and $\alpha_{\text{ox}}(\text{corr})$ or $\Delta\alpha_{\text{ox}}(\text{corr})$, as $\Delta\alpha_{\text{ox}}$ is composed of the contributions of absorption and of $\Delta\alpha_{\text{ox}}(\text{corr})$.

In passing, we note that lack of correlations between the X-ray absorption column density and UV properties does not necessarily contradict with the scenario of radiatively accelerated wind as naively thought. For locally optically thin material, the ratio of the radiation force to the gravitational force is a function of Eddington ratio and the cross-section ratio of effective absorption to Thomson scattering. If resonant scattering is responsible for the absorption opacity, the cross-section will be determined by the fraction Li-like ions. According to the equatorial wind model(Murray et al. 1995), a clump of highly ionized gas (shielding gas), which accounts for most X-ray opacity, blocks the soft X-ray interior to the wind. The transmitted flux of soft X-rays that ionize Li-like ions in the wind depends strongly on the X-ray column density, N_{H} . If N_{H} along the direction is very small, high-

velocity wind cannot be launched because of the reduction of the radiation force caused by the over-ionization. On the other hand, if N_{H} is very large, the wind will end up with a turbulent flow due to the blocking of thick very-low-ionized gas behind (see the figure 4 of Proga et al. 2000). Thus, high-velocity wind can only be launched when the radial column density N_{H} is moderate as the fraction of Li-like ions, such as C IV and N V, is large enough. As far as the X-ray absorption column density is in the right range, the fraction of Li-like ions should be the dominant species. The flow properties are then determined self-consistently by the launching radius, the gas density at the launching radius and the radiation intensity. If X-ray absorber is well separated from the UV absorber, then we would not expect any correlation between the X-ray absorption column density and the flow properties for BAL QSOs apart.

On the other hand, the X-ray absorber may be the ‘hitchhiking’ gas just located at the inner edge of the wind, and its properties may have a close connection with the boundary conditions of the disk wind (Murray et al. 1995). In that case, we should consider globally the structure of gas along a line of sight. The wind starts at a radius where the radiation force is substantially larger than the gravitational force. As far as the gas density is high enough, such a region can certainly exist. Murray et al. (1995) has worked out a consistent line acceleration model, and they found that gas column density and final velocity are correlated for a constant Eddington ratio and at a given launch radius. However, if the launching radius is not exactly scaled with luminosity as $L^{1/2}$ and there are a range of Eddington ratio, as they assumed, the correlation can be smeared out.

More interesting results of our work are the strong correlations between the parameters of outflow and intrinsic α_{ox} . We argue that these correlations are essential rather than due to some selection effect or the secondary effect of other correlations (see previous subsection for details). In fact our results are consistent with Richards (2006) who found that the QSOs with large blueshifts of C IV emission line, i.e. the parent population of BAL QSOs as suggested by Richards (2006), tend to have lower X-ray luminosity for given optical luminosity (their figure 5). It is also upheld by Laor & Brandt (2002) who presented significant correlation between the equivalent width of C IV absorption and α_{ox} in a sample of non-BAL QSOs. This correlation is actually predicted by Murray et al. (1995), in which they found that quasars with a large X-ray to UV ratio can only produce weak low velocity winds while quasars with a small X-ray to UV ratio can produce strong and large velocity winds. This is exactly what we have found here. As we discussed above, their model also predicted a correlation between the X-ray absorption column density and the maximum velocity of the flow, which is not observed in this sample. Lack of such correlation may be due to two important factors that (1) variation in the Eddington ratio and launching radius; (2) the large uncertainties in the measurement of absorption column density.

We do not fully understand why the variation in the Eddington ratio and launching does not completely smear out the correlation with $\alpha_{\text{ox}}(\text{corr})$. There seems one reason for this. Wang et al. (2004) found that the 2-10keV luminosities to bolometric luminosities ratio tightly anti-correlated with Eddington ratio for a sample of broad-line and narrow-line Seyfert 1 AGNs. If this correlation holds up for BAL QSOs, one would expect that quasars with high Eddington ratio would have larger radiative acceleration force, or large terminal velocity, and at the same time X-ray weaker. Ganguly et al. (2007) find that v_{max} as a function of Eddington ratio has an upper envelope in the SDSS3 BAL catalog, exactly as expected. Since there is no clear correlation of BI with UV luminosities (cf. Laor & Brandt 2002), Eddington rate and black hole mass (Ganguly et al. 2007), it is very likely that the BAL properties are more likely determined by the SED of quasars rather than Eddington ratio.

5. SUMMARY

We compile a large C IV BAL QSOs sample from the *XMM-Newton* archive data and SDSS DR5. The sample consists of 41 BAL QSOs, among which 26 QSOs are detected in the X-ray band. Our sample spans wide and homogeneous ranges of both BI and v_{max} and can be used to complement the LBQS/*Chandra* BAL sample (G06). In addition, the combined sample of ours and G06s show a more homogeneous distribution of intrinsic X-ray properties than G06s. Using this combined sample, we investigate the correlations between X-ray and UV properties of BAL QSOs.

We briefly summarize our conclusions below:

1. We confirm the previous results that BAL QSOs are generally soft X-ray weak, which is mainly due to the intrinsic X-ray absorption. We also find the X-ray luminosities of BAL QSOs with given optical luminosity have large scatter. The scatter is caused by both the various column densities of X-ray absorber and the scatter of intrinsic X-ray emission at given optical luminosity.
2. We do not find any evidence for the claimed correlation between the BAL properties and soft X-ray absorption, with an exception of the correlation between BI and $\Delta\alpha_{\text{ox}}$. The correlation between BI and $\Delta\alpha_{\text{ox}}$ can be induced by the correlation between BI and the intrinsic α_{ox} . The X-ray absorber is important for launching the high-velocity wind but do not directly determine the BAL properties.
3. There are significant correlations between intrinsic X-ray strength, $\alpha_{\text{ox}}(\text{corr})$, and BI and v_{max} in the combined sample. These correlations are essential rather than due

to any artificiality. We preliminarily interpret that the BAL properties are influenced by the intrinsic SED of QSOs, which is consistent with the prediction of a radiatively accelerated disk wind model (Murray et al. 1995).

We thank the anonymous referee for helpful comments. We thank Paul Hewett for providing electronic data of LBQS spectra. We also acknowledge the Sloan Digital Sky Survey (<http://www.sdss.org>). This work was supported by the Knowledge Innovation Program of the Chinese Academy of Sciences, Grant No. KJCX2-YW-T05 and the National Basic Research Program of China (973 Program) under Grant No. 2007CB815400.

REFERENCES

- Adelman-McCarthy, J. K., et al. 2008, *ApJS*, 175, 297
- Aldcroft, T. L. & Green, P. J., 2003, *ApJ*, 592, 710
- Arnaud, K. A., 1996, in ASP Conf. Ser. 101: *Astronomical Data Analysis Software and Systems V*, eds. G. Jacoby & J. Barnes vol. 5, 17
- Avni, Y., & Tananbaum, H. 1986, *ApJ*, 305, 83
- Bade, N., Siebert, J., Lopez, S., Voges, W., & Reimers, D. 1997, *A&A*, 317, L13
- Baskin, A., & Laor, A. 2004, *MNRAS*, 350, L31
- Boroson, T. A., & Meyers, K. A. 1992, *ApJ*, 397, 442
- Brandt, W. N., Laor, A., & Wills, B. J. 2000, *ApJ*, 528, 637
- Brinkmann, W., Wang, T., Matsuoka, M., & Yuan, W. 1999, *A&A*, 345, 43
- Brotherton, M. S., De Breuck, C., & Schaefer, J. J. 2006, *MNRAS*, 372, L58
- Cash, W., 1979, *ApJ*, 228, 939
- Chaffee, F. H., Foltz, C. B., Hewett, P. C., Francis, P. A., Weymann, R. J., Morris, S. L., Anderson, S. F., & MacAlpine, G. M. 1991, *AJ*, 102, 461
- Chartas, G., Brandt, W. N. & Gallagher, S. C., 2003, *ApJ*, 595, 85
- Chartas, G., Brandt, W. N., Gallagher, S. C. & Garmire, G. P., 2002, *ApJ*, 579, 169

- Dickey, J. M. & Lockman, F. J., 1990, *ARA&A*, 28, 385
- Foltz, C. B., Chaffee, F. H., Jr., Hewett, P. C., MacAlpine, G. M., Turnshek, D. A., Weymann, R. J., & Anderson, S. F. 1987, *AJ*, 94, 1423
- Foltz, C. B., Chaffee, F. H., Hewett, P. C., Weymann, R. J., Anderson, S. F., & MacAlpine, G. M. 1989, *AJ*, 98, 1959
- Gallagher, S. C., Brandt, W. N., Sambruna, R. M., Mathur, S., & Yamasaki, N. 1999, *ApJ*, 519, 549
- Gallagher, S. C., Brandt, W. N., Chartas, G. & Garmire, G. P., 2002, *ApJ*, 567, 37
- Gallagher, S. C., Brandt, W. N., Chartas, G., Priddey, R., Garmire, G. P., & Sambruna, R. M. 2006, *ApJ*, 644, 709
- Gallagher, S. C., Brandt, W. N., Wills, B. J., Charlton, J. C., Chartas, G., & Laor, A. 2004, *ApJ*, 603, 425
- Ganguly, R., Brotherton, M. S., Cales, S., Scoggins, B., Shang, Z., & Vestergaard, M. 2007, *ApJ*, 665, 990
- Gehrels, N., 1986, *ApJ*, 303, 336
- George, I. M., Turner, T. J., Yaqoob, T., Netzer, H., Laor, A., Mushotzky, R. F., Nandra, K., & Takahashi, Y., 2000, *ApJ*, 531, 52
- Green, P. J., et al. 1995, *ApJ*, 450, 51
- Grupe, D., Mathur, S., & Elvis, M., 2003, *AJ*, 126, 1159
- Hewett, P. C., & Foltz, C. B. 2003, *AJ*, 125, 1784
- Hewett, P. C., Foltz, C. B., & Chaffee, F. H. 1995, *AJ*, 109, 1498
- Hewett, P. C., Foltz, C. B., Chaffee, F. H., Francis, P. J., Weymann, R. J., Morris, S. L., Anderson, S. F., & MacAlpine, G. M. 1991, *AJ*, 101, 1121
- Ivezić, Ž., et al. 2002, *AJ*, 124, 2364
- Kraft, R. P., Burrows, D. N., & Nousek, J. A., 1991, *ApJ*, 374, 344
- Laor, A., & Brandt, W. N. 2002, *ApJ*, 569, 641

- Morris, S. L., Weymann, R. J., Anderson, S. F., Hewett, P. C., Francis, P. J., Foltz, C. B., Chaffee, F. H., & MacAlpine, G. M. 1991, *AJ*, 102, 1627
- Morrison, R. & McCammon, D., 1983, *ApJ*, 270 ,119
- Murray, N., Chiang, J., Grossman, S. A., & Voit, G. M. 1995, *ApJ*, 451, 498
- Ogle, P. M., Cohen, M. H., Miller, J. S., Tran, H. D., Goodrich, R. W., & Martel, A. R. 1999, *ApJS*, 125, 1
- Page, K. L., Reeves, J. N., O'Brien, P. T., & Turner, M. J. L., 2005, *MNRAS*, 365, 898
- Park, T., Kashyap, V. L., Siemiginowska, A., van Dyk, D. A., Zezas, A., Heinke, C., & Wargelin, B. J. 2006, *ApJ*, 652, 610
- Proga, D., Stone, J. M., & Kallman, T. R. 2000, *ApJ*, 543, 686
- Reeves, J. N. & Turner, M. J. L., 2000, *MNRAS*, 316, 234
- Reichard, T. A., et al. 2003, *AJ*, 125, 1711
- Richards, G. T. 2006, *ArXiv Astrophysics e-prints*, arXiv:astro-ph/0603827
- Shemmer, O., Brandt, W. N., Gallagher, S. C., Vignali, C., Boller, T., Chartas, G., & Comastri, A. 2005, *AJ*, 130, 2522
- Steffen, A. T., Strateva, I., Brandt, W. N., Alexander, D. M., Koekemoer, A. M., Lehmer, B. D., Schneider, D. P., & Vignali, C. 2006, *AJ*, 131, 2826
- Strateva, I. V., Brandt, W. N., Schneider, D. P., Vanden Berk, D. G., & Vignali, C. 2005, *AJ*, 130, 387
- Tananbaum, H., et al. 1979, *ApJ*, 234, L9
- Tang, S. M., Zhang, S. N., & Hopkins, P. F. 2007, *MNRAS*, 377, 1113
- Trump, J. R., et al. 2006, *ApJS*, 165, 1
- Vanden Berk, D. E., et al. 2001, *AJ*, 122, 549
- Wang, J., Jiang, P., Zhou, H., Wang, T., Dong, X., & Wang, H. 2008, *ApJ*, 676, L97
- Wang, J.-M., Watarai, K.-Y., & Mineshige, S. 2004, *ApJ*, 607, L107
- Wang, T. G., Brinkmann, W., Yuan, W., Wang, J. X., & Zhou, Y. Y. 2000, *ApJ*, 545, 77
- Wang, T. G., Wang, J. X., Brinkmann, W., & Matsuoka, M. 1999, *ApJ*, 519, L35

- Wang, H.-Y., Wang, T.-G., & Wang, J.-X. 2005, *ApJ*, 634, 149
- Wang, H.-Y., Wang, T.-G., & Wang, J.-X. 2007, *ApJS*, 168, 195
- Weymann,R.J., Morris,S.L.,Foltz,C.B.,& Hewett,P.C., 1991,*ApJ*,373,23
- White, R. L., Becker, R. H., Helfand, D. J., & Gregg, M. D. 1997, *ApJ*, 475, 479
- Wilkes, B. J., Tananbaum, H., Worrall, D. M., Avni, Y., Oey, M. S., & Flanagan, J. 1994, *ApJS*, 92, 53
- Yuan, W., Siebert, J., & Brinkmann, W. 1998,*A&A*, 334, 498
- Zhou, H., Wang, T., Wang, H., Wang, J., Yuan, W., & Lu, Y. 2006, *ApJ*, 639, 716

Table 1. Observed BAL QSOs

Name(SDSS) ^a	z^b	i^c	f_{2500}^d	N_H^e	BI ^f	v_{\max}^g	BAL Type ^h	R_t^i
J020230.66-075341.2	1.722	18.69	4.69	2.13	245	6518	Hi	< 0.68
J023224.87-071910.5	1.597	18.14	9.81	3.02	450	7855	Hi	< 0.44
J024304.68+000005.4	1.995	18.19	7.96	3.56	360	5847	Hi	< 0.81
J085551.24+375752.2	1.929	18.19	8.98	2.92	268	20777	Hi	< 0.40
J090928.50+541925.9	3.760	19.58	1.02	2.09	2890	12086	H	< 0.97
J091127.61+055054.1	2.793	17.77	11.38	3.64	296	20368	H	< 0.32
J091400.95+410600.9	2.052	19.51	2.10	1.80	258	18625	Hi	< 0.92
J092138.45+301546.9	1.590	17.97	9.77	1.90	264	12479	Hi	< 0.41
J092238.43+512121.2	1.753	20.11	1.36	1.43	900	10823	Lo	< 1.14
J092345.19+512710.0	2.168	19.14	3.18	1.42	1832	18755	Hi	1.42
J092507.54+521102.6	2.995	19.10	4.22	1.46	2982	14990	H	< 0.80
J094309.56+481140.5	1.809	18.72	5.43	1.21	106	22401	Hi	< 0.59
J094440.42+041055.6	1.984	18.23	7.42	3.63	1934	15095	Lo	< 0.50
J095110.56+393243.9	1.716	19.68	1.97	1.57	2328	11371	Hi	< 1.07
J100728.69+534326.7	1.772	19.06	3.37	0.74	3	6656	Hi	< 0.80
J105201.35+441419.8	1.791	18.47	5.06	1.12	617	10192	Hi	< 0.55
J110853.98+522337.9	1.665	18.53	5.81	0.90	87	7266	Hi	< 0.55
J111816.95+074558.1	1.735	15.89	64.89	3.53	5	5306	Hi	< -0.45
J112055.78+431412.5	2.389	18.66	4.22	2.07	3684	20103	H	< 0.64
J112432.14+385104.3	3.530	19.99	1.75	2.06	236	12438	H	< 1.24
J113419.96+485805.7	3.080	20.05	2.29	1.60	1988	19192	H	< 1.26
J113406.87+525959.0	1.769	18.84	4.71	1.11	1046	8581	Hi	< 0.67
J120449.77+020635.6	2.776	19.24	3.43	1.88	518	19690	H	< 0.85
J120522.18+443140.4	1.921	18.42	5.62	1.27	772	22284	Hi	< 0.57
J122708.29+012638.4	1.954	19.07	2.94	1.84	835	19612	Hi	< 1.58
J125741.41+565214.2	1.841	19.36	2.59	1.27	1811	18178	Hi	< 1.00
J132827.07+581836.9	3.140	18.53	3.49	1.37	85	6323	H	< 0.27
J133004.72+472301.0	2.825	19.16	2.38	1.55	4020	17357	H	1.18
J133553.61+514744.1	1.838	18.08	7.48	1.11	486	9359	Lo	1.14
J133639.40+514605.2	2.229	19.04	2.65	1.11	2319	8631	Hi	< 0.80
J134145.12-003631.0	2.215	18.52	5.86	2.06	1519	8085	Lo	< 0.58
J142555.22+373900.7	2.731	19.13	2.69	0.94	53	24676	H	< 0.55
J142539.38+375736.7	1.897	18.02	8.52	0.95	190	24464	Hi	< 0.08
J142652.94+375359.9	1.812	19.12	3.43	0.95	43	20131	Hi	< 0.57

Table 1—Continued

Name(SDSS) ^a	z ^b	i ^c	f_{2500} ^d	N_{H} ^e	BI ^f	v_{max} ^g	BAL Type ^h	R_i ⁱ
J144027.00+032637.9	2.136	18.74	4.05	2.77	1141	20041	Lo	< 0.68
J144625.48+025548.6	1.883	18.97	4.31	3.06	360	6665	Hi	< 0.71
J150824.22-000603.8	1.578	18.44	6.73	4.58	192	10208	Hi	< 0.51
J152553.89+513649.1	2.883	16.57	29.85	1.57	754	17965	H	< -0.46
J153229.97+323658.4	3.048	19.22	1.94	2.03	2614	14090	H	< 0.85
J154359.44+535903.2	2.370	16.96	19.76	1.25	29	13292	H	< -0.11
J164151.84+385434.2	3.776	18.51	7.56	1.21	4610	> 25000	H	< 0.57

^aSDSS ID.

^bredshift.

^c i band fiber magnitude of SDSS.

^dThe rest-frame 2500Å flux density(in units of 10^{-17} erg cm⁻² s⁻¹ Å⁻¹).

^eThe values for N_{H} (in units of 10^{20} cm⁻²) are from Galactic HI maps (Dickey & Lockman 1990).

^fThe BALnicity Index (BI; in units of km s⁻¹)

^gThe maximum outflow velocity(v_{max} ; in units of km s⁻¹)

^hThe BAL subtype. “Hi” denotes a HiBAL-only object; “Lo” denotes a LoBAL detected through Mg II absorption; “H” denotes a HiBAL object in which the Mg II region is not within the spectral coverage.

ⁱThe radio-to-optical flux ratios, $R_i = \log(S_{1.4\text{GHz}}/S_i)$, following the definition of Ivezić et al. (2002).

Table 2. *XMM-Newton* Observing Log

Name(SDSS)	Obs.ID ^a	Date	T_{exp} ^b	Instrument	Soft ^c	Hard ^c	Counts Rate ^d	HR ^e
J020230.66-075341.2	0411980201	2006-07-03	8.16	pn	< 7.9	< 16.5	< 1.81	...
J023224.87-071910.5	0200730401	2004-01-07	37.51	pn	$64^{+17.6}_{-15.8}$	$35^{+15.6}_{-13.8}$	$2.64^{+0.62}_{-0.57}$	$-0.29^{+0.17}_{-0.19}$
J024304.68+000005.4	0111200101	2000-07-29	38.51	mos1	$76^{+19.3}_{-17.5}$	$54^{+17.0}_{-15.2}$	$3.39^{+0.66}_{-0.61}$	$-0.17^{+0.13}_{-0.12}$
J085551.24+375752.2	0302581801	2005-10-10	28.45	mos1	$48^{+16.4}_{-14.7}$	$12^{+12.9}_{-11.5}$	$2.11^{+0.77}_{-0.71}$	$-0.60^{+0.05}_{-0.18}$
J090928.50+541925.9	0200960101	2005-03-28	71.05	mos2	< 18.0	< 22.3	< 0.40	...
J091127.61+055054.1	0083240201(T)	2001-11-02	8.93	pn	$277^{+35.9}_{-34.2}$	$151^{+31.1}_{-29.2}$	$47.94^{+5.24}_{-5.10}$	$-0.29^{+0.08}_{-0.08}$
J091400.95+410600.9	0147671001	2003-04-27	13.37	mos1	< 5.8	< 8.6	< 0.72	...
J092138.45+301546.9	0150620101	2003-04-23	15.76	mos1	$11^{+8.7}_{-6.8}$	< 23.4	$1.59^{+0.79}_{-0.68}$	< 0.35
J092238.43+512121.2	0300910301	2005-10-08	15.57	pn	$173^{+27.5}_{-25.7}$	< 13.8	$10.73^{+2.02}_{-1.91}$	< -0.85
J092345.19+512710.0	0300910301	2005-10-08	15.55	pn	$31^{+17.3}_{-15.6}$	< 9.8	$0.32^{+1.54}_{-0.31}$	< -0.52
J092507.54+521102.6	0201130501	2004-11-15	46.54	mos1	$45^{+13.8}_{-12.0}$	< 29.5	$1.35^{+0.38}_{-0.34}$	< -0.21
J094309.56+481140.5	0201470101	2004-10-14	30.35	mos1	< 14.6	< 25.2	< 0.95	...
J094440.42+041055.6	0201290301	2004-05-18	21.27	mos1	< 6.5	< 11.1	< 0.50	...
J095110.56+393243.9	0111290101	2001-11-03	21.10	mos1	< 11.1	< 11.7	< 0.77	...
J100728.69+534326.7	0070340201	2001-05-10	19.69	pn	$135^{+24.1}_{-22.3}$	$43^{+17.3}_{-15.5}$	$9.04^{+1.49}_{-1.40}$	$-0.52^{+0.11}_{-0.12}$
J105201.35+441419.8	0146990901	2003-05-24	5.11	pn	$32^{+12.2}_{-10.4}$	$25^{+13.1}_{-11.2}$	$11.16^{+3.42}_{-3.06}$	$-0.12^{+0.23}_{-0.25}$
J110853.98+522337.9	0304071201	2005-10-21	8.18	mos2	< 21.3	< 8.1	< 3.09	...
J111816.95+074558.1	0203560401(T)	2004-06-26	68.34	pn	$8762^{+162.2}_{-161.8}$	$2598^{+93.9}_{-92.1}$	$166.24^{+2.79}_{-2.69}$	$-0.54^{+0.01}_{-0.01}$
J112055.78+431412.5	0107860201	2001-05-08	21.96	mos1	< 5.8	< 13.4	< 0.57	...
J112432.14+385104.3	0052140201	2001-12-03	24.55	pn	$31^{+14.8}_{-13.0}$	< 20.4	$1.63^{+0.80}_{-0.72}$	< -0.21
J113419.96+485805.7	0149900201	2003-11-24	14.96	pn	< 13.6	< 17.5	< 1.43	...
J113406.87+525959.0	0200431301	2004-11-04	10.82	mos2	$2^{+6.9}_{-1.8}$	< 10.4	$0.52^{+0.80}_{-0.51}$	< 0.70
J120449.77+020635.6	0093060101	2001-12-21	14.21	mos1	< 11.6	< 7.4	< 0.99	...
J120522.18+443140.4	0156360101	2003-06-11	23.95	pn	$92^{+22.2}_{-20.3}$	$47^{+21.0}_{-19.2}$	$5.80^{+1.26}_{-1.18}$	$-0.32^{+0.17}_{-0.20}$
J122708.29+012638.4	0110990201	2001-06-23	9.56	pn	$22^{+14.0}_{-12.2}$	< 12.4	$2.51^{+1.79}_{-1.60}$	< -0.28
J125741.41+565214.2	0081340201	2001-06-07	21.39	mos1	$4^{+6.5}_{-4.0}$	< 6.1	$0.12^{+0.42}_{-0.12}$	< 0.18
J132827.07+581836.9	0405690201	2006-11-19	25.97	pn	$27^{+18.5}_{-16.7}$	< 27.6	$1.42^{+1.03}_{-0.97}$	< 0.00
J133004.72+472301.0	0112840201	2003-01-15	17.11	pn	< 12.3	< 7.9	< 0.69	...
J133553.61+514744.1	0084190201	2002-06-12	38.39	pn	$86^{+26.0}_{-24.3}$	$6^{+21.2}_{-5.9}$	$2.40^{+0.90}_{-0.84}$	$-0.87^{+0.11}_{-0.13}$
J133639.40+514605.2	0084190201	2002-06-12	37.24	pn	< 44.7	< 10.2	< 0.78	...
J134145.12-003631.0	0111281601	2002-07-20	7.41	mos1	$2^{+5.3}_{-2.0}$	< 5.0	$0.23^{+0.90}_{-0.23}$	< 0.40
J142555.22+373900.7	0112230201	2002-12-18	19.48	pn	$29^{+13.0}_{-11.2}$	< 28.6	$2.34^{+0.89}_{-0.80}$	< -0.01
J142539.38+375736.7	0112230201	2002-12-18	19.48	pn	$109^{+24.2}_{-22.5}$	$36^{+19.4}_{-17.6}$	$7.44^{+1.57}_{-1.49}$	$-0.50^{+0.15}_{-0.20}$
J142652.94+375359.9	0112230201	2002-12-18	19.48	pn	$14^{+14.5}_{-13.2}$	< 32.9	$1.61^{+1.15}_{-1.05}$	< 0.41

Table 2—Continued

Name(SDSS)	Obs.ID ^a	Date	T_{exp} ^b	Instrument	Soft ^c	Hard ^c	Counts Rate ^d	HR ^e
J144027.00+032637.9	0300210701	2006-01-08	23.05	mos1	< 19.5	< 17.7	< 1.08	...
J144625.48+025548.6	0203050801	2005-01-12	7.86	mos1	< 3.1	$4^{+5.4}_{-3.9}$	$0.13^{+0.82}_{-0.13}$	> 0.13
J150824.22-000603.8	0305750201	2005-07-20	5.03	mos2	$6^{+6.3}_{-4.5}$	< 11.3	$2.18^{+1.65}_{-1.29}$	< 0.34
J152553.89+513649.1	0011830401(T)	2001-12-13	2.82	pn	$122^{+24.7}_{-22.9}$	$56^{+18.6}_{-16.9}$	$63.05^{+10.86}_{-10.17}$	$-0.37^{+0.12}_{-0.13}$
J153229.97+323658.4	0039140101	2002-07-30	4.74	pn	< 8.7	< 11.7	< 2.97	...
J154359.44+535903.2	0060370901(T)	2002-02-06	16.18	pn	$571^{+43.1}_{-41.5}$	$115^{+24.8}_{-22.9}$	$42.40^{+3.06}_{-2.93}$	$-0.66^{+0.04}_{-0.05}$
J164151.84+385434.2	0204340101	2004-08-20	12.22	pn	< 7.7	< 17.0	< 1.27	...

^a(T) means the object is the intended PI target of the *XMM-Newton* observation.

^bThe effective exposure time in 10^3 s.

^cErrors are 1σ Poisson errors(Gehrels 1986) for detections,and for non-detections the limits are the 90% confidence limits from Bayesian statistics(Kraft et al. 1991).The count rate is the full energy band,0.3-10.0keV.

^dThe count rate in 10^{-3} counts s^{-1}

^e*HR* is defined as $(h - s)/(h + s)$.The *HR* errors are propagated from the counts errors using the Bayesian estimation of Park et al. (2006).Notice the difference of the definitions of the hard and soft band between ours(s : 0.3 – 2.0 keV; h : 2.0 – 10.0 keV) and G06s(s : 0.5 – 2.0 keV; h : 2.0 – 8.0 keV).

Table 3. X-RAY PROPERTIES

Name(SDSS)	N_H^a	Γ_{HR}^b	$\log(f_x)^c$	$\log(f_{2kev})^d$	$\log(f_{2500})^d$	$\log(l_{2500})^e$	α_{ox}	$\Delta\alpha_{ox}^f$	$\alpha_{ox}(corr)^g$	$\Delta\alpha_{ox}(corr)^h$
J020230.66–075341.2	< -13.418	< -31.782	-27.140	30.726	< -1.78	< -0.22	< -1.34	< 0.22
J023224.87–071910.5	$2.96^{+1.76}_{-1.14}$	$1.06^{+0.32}_{-0.26}$	-13.230	-31.547	-26.861	30.945	-1.80	-0.21	-1.57	0.02
J024304.68+000005.4	$4.69^{+4.34}_{-2.42}$	$1.12^{+0.21}_{-0.22}$	-13.095	-31.376	-26.827	31.155	-1.75	-0.13	-1.50	0.12
J085551.24+375752.2	$0.58^{+1.00}_{-0.56}$	$1.93^{+0.52}_{-0.12}$	-13.576	-31.331	-26.794	31.162	-1.74	-0.12	-1.73	-0.11
J090928.50+541925.9	< -13.814	< -32.178	-27.316	31.129	< -1.87	< -0.25	< -1.42	< 0.20
J091127.61+055054.1	$1.89^{+1.58}_{-1.01}$	$1.22^{+0.13}_{-0.11}$	-12.620	-30.787	-26.467	31.768	-1.66	...	-1.41	...
J091400.95+410600.9	< -13.537	< -31.902	-27.390	30.613	< -1.73	< -0.19	< -1.34	< 0.21
J092138.45+301546.9	< 21.25	> 0.21	-13.137	-32.144	-26.864	30.939	> -2.03	> -0.44	< -1.51	< 0.09
J092238.43+512121.2	< 0.01	> 2.38	-13.560	-31.205	-27.669	30.212	> -1.36	> 0.13	< -1.47	< 0.03
J092345.19+512710.0	< 1.50	> 1.47	-14.155	-32.167	-27.177	30.869	> -1.92	> -0.33	< -1.43	< 0.16
J092507.54+521102.6	< 5.11	> 1.12	-13.463	-31.721	-26.852	31.433	> -1.87	> -0.21	< -1.56	< 0.10
J094309.56+481140.5	< -13.436	< -31.803	-27.049	30.856	< -1.83	< -0.25	< -1.45	< 0.14
J094440.42+041055.6	< -13.571	< -31.931	-26.861	31.116	< -1.95	< -0.33	< -1.53	< 0.09
J095110.56+393243.9	< -13.651	< -32.017	-27.518	30.346	< -1.73	< -0.22	< -1.39	< 0.13
J100728.69+534326.7	$2.39^{+2.24}_{-1.19}$	$1.42^{+0.24}_{-0.19}$	-13.131	-31.206	-27.268	30.621	-1.51	0.04	-1.37	0.18
J105201.35+441419.8	$14.07^{+8.61}_{-5.09}$	$0.89^{+0.37}_{-0.33}$	-13.012	-31.464	-27.086	30.811	-1.68	-0.11	-1.38	0.19
J110853.98+522337.9	< -12.834	< -31.201	-27.065	30.775	< -1.59	< -0.02	< -1.38	< 0.19
J111816.95+074558.1	$0.36^{+0.06}_{-0.06}$	$1.64^{+0.02}_{-0.02}$	-12.228	-30.155	-25.995	31.877	-1.60	...	-1.51	...
J112055.78+431412.5	< -13.599	< -31.963	-26.995	31.124	< -1.91	< -0.29	< -1.46	< 0.15
J112432.14+385104.3	< 5.48	> 1.03	-13.840	-32.175	-27.126	31.276	> -1.94	> -0.30	< -1.56	< 0.08
J113419.96+485805.7	< -13.816	< -32.182	-27.100	31.205	< -1.95	< -0.32	< -1.50	< 0.13
J113406.87+525959.0	< 45.73	> -0.48	-13.158	-32.835	-27.123	30.765	> -2.19	> -0.63	< -1.37	< 0.20
J120449.77+020635.6	< -13.251	< -31.616	-26.992	31.238	< -1.78	< -0.14	< -1.43	< 0.20
J120522.18+443140.4	$1.77^{+2.50}_{-1.22}$	$1.16^{+0.33}_{-0.24}$	-13.422	-31.666	-27.000	30.952	-1.79	-0.20	-1.57	0.03
J122708.29+012638.4	< 5.86	> 1.14	-13.842	-32.099	-27.272	30.694	> -1.85	> -0.30	< -1.56	< 0.00
J125741.41+565214.2	< 15.81	> 0.40	-13.959	-32.827	-27.361	30.558	> -2.10	> -0.56	< -1.44	< 0.10
J132827.07+581836.9	< 37.22	> 0.67	-13.540	-32.228	-26.904	31.415	> -2.04	> -0.39	< -1.53	< 0.13
J133004.72+472301.0	< -14.098	< -32.464	-27.140	31.103	< -2.04	< -0.43	< -1.64	< -0.02
J133553.61+514744.1	$1.41^{+3.70}_{-1.24}$	$2.56^{+2.04}_{-0.45}$	-14.048	-31.642	-26.901	31.017	-1.82	-0.22	-1.96	-0.36
J133639.40+514605.2	< -14.084	< -32.451	-27.239	30.828	< -2.00	< -0.42	< -1.67	< -0.09
J134145.12–003631.0	< 37.45	> -0.01	-13.475	-32.773	-26.899	31.163	> -2.26	> -0.63	< -1.43	< 0.20
J142555.22+373900.7	< 28.69	> 0.70	-13.413	-32.058	-27.108	31.110	> -1.90	> -0.29	< -1.44	< 0.17
J142539.38+375736.7	$2.90^{+1.68}_{-1.17}$	$1.49^{+0.46}_{-0.26}$	-13.246	-31.267	-26.826	31.117	-1.71	-0.09	-1.57	0.05
J142652.94+375359.9	< 31.55	> 0.04	-13.358	-32.551	-27.248	30.659	> -2.04	> -0.48	< -1.41	< 0.14

Table 3—Continued

Name(SDSS)	N_H^a	Γ_{HR}^b	$\log(f_x)^c$	$\log(f_{2keV})^d$	$\log(f_{2500})^d$	$\log(l_{2500})^e$	α_{ox}	$\Delta\alpha_{ox}^f$	$\alpha_{ox}(corr)^g$	$\Delta\alpha_{ox}(corr)^h$
J144027.00+032637.9	< -13.617	< -31.980	-27.081	30.953	< -1.88	< -0.29	< -1.52	< 0.07
J144625.48+025548.6	> 13.56	< 0.56	-14.079	-32.807	-27.126	30.811	< -2.18	< -0.61	-1.47	0.11
J150824.22-000603.8	< 20.29	> 0.24	-12.869	-31.846	-27.030	30.767	> -1.85	> -0.28	< -1.32	< 0.24
J152553.89+513649.1	$5.36^{+8.61}_{-3.28}$	$1.33^{+0.22}_{-0.19}$	-12.556	-30.636	-26.028	32.230	-1.77	0.00	-1.55	0.22
J153229.97+323658.4	< -13.615	< -31.980	-27.179	31.119	< -1.84	< -0.23	< -1.39	< 0.22
J154359.44+535903.2	$1.11^{+0.42}_{-0.35}$	$1.79^{+0.12}_{-0.08}$	-12.889	-30.684	-26.330	31.783	-1.67	0.03	-1.63	0.08
J164151.84+385434.2	< -13.961	< -32.327	-26.444	32.004	< -2.26	< -0.52	< -1.73	< 0.00

^aIntrinsic absorption column density in units of 10^{22}cm^{-2} , its value or upper or lower limit is determined by fitting the observed spectrum, or comparing the observed HR to a simulated HR that takes the instrument response into account, or the upper limit of count rates, assuming $\Gamma = 2.0$ and a simple neutral absorption.

^b Γ_{HR} , following the definition of G06s, is a coarse measure of the hardness of the X-ray spectrum determined by comparing the observed HR to a simulated HR that takes the instrument response into account.

^cThe full-band X-ray flux, f_x , has units of $\text{erg cm}^{-2} \text{s}^{-1}$.

^dX-ray and optical flux densities were measured at rest-frame 2 keV and 2500 Å, respectively; units are $\text{erg cm}^{-2} \text{s}^{-1} \text{Hz}^{-1}$.

^eThe 2500 Å monochromatic luminosity, l_{2500} , has units of $\text{erg s}^{-1} \text{Hz}^{-1}$. The redshift bandpass correction has been included.

^fThe parameter $\Delta\alpha_{ox}$ is the difference between the observed α_{ox} and $\alpha_{ox}(l_{2500})$, the predicted α_{ox} from l_{2500} calculated from Equation 6 of (Strateva et al. 2005).

^gThe parameter $\alpha_{ox}(corr)$ is α_{ox} calculated assuming $\Gamma = 2.0$ and using the hard-band count rate to normalize the X-ray continuum.

^h $\Delta\alpha_{ox}(corr) = \alpha_{ox}(corr) - \alpha_{ox}(l_{2500})$.

Table 4. Results from Non-Parametric Bivariate Statistical Tests

Variables ^a Independent/Dependent	Generalized Kendall		ρ	Spearman Prob. ^b (%)
	τ	Prob. ^b (%)		
$N_{\text{H}}/\Delta\alpha_{\text{ox}}(51)$	6.930	< 0.01
$N_{\text{H}}/\Delta\alpha_{\text{ox}}(\text{corr})(51)$	0.913	36.2
$N_{\text{H}}/\text{BI}(53)$	2.296	2.2
$N_{\text{H}}/v_{\text{max}}(53)$	0.365	71.5
$\Delta\alpha_{\text{ox}}/\text{BI}(74)$	3.467	0.05
$\Delta\alpha_{\text{ox}}/v_{\text{max}}(74)$	2.003	4.5
$\Delta\alpha_{\text{ox}}/\text{BI}(\text{HiBALs only } 45)$	2.553	1.1
$\Delta\alpha_{\text{ox}}/v_{\text{max}}(\text{HiBALs only } 45)$	0.414	67.9
$\alpha_{\text{ox}}(\text{corr})/\text{BI}(74)$	3.657	0.03	−0.384	0.1
$\alpha_{\text{ox}}(\text{corr})/v_{\text{max}}(74)$	3.936	0.01	−0.458	0.01
$\alpha_{\text{ox}}(\text{corr})/\text{BI}(\text{HiBALs only } 45)$	3.447	0.06	−0.492	0.1
$\alpha_{\text{ox}}(\text{corr})/v_{\text{max}}(\text{HiBALs only } 45)$	3.335	0.09	−0.469	0.2
$\Delta\alpha_{\text{ox}}(\text{corr})/\text{BI}(74)$	3.215	0.1	−0.329	0.5
$\Delta\alpha_{\text{ox}}(\text{corr})/v_{\text{max}}(74)$	3.623	0.03	−0.425	0.03
$\Delta\alpha_{\text{ox}}(\text{corr})/\text{BI}(\text{HiBALs only } 45)$	3.071	0.2	−0.430	0.4
$\Delta\alpha_{\text{ox}}(\text{corr})/v_{\text{max}}(\text{HiBALs only } 45)$	3.218	0.1	−0.473	0.2

^aThe number of data points is given in parentheses.

^bThe probability(in units of percent) that the given variables are not correlated. Spearman’s ρ cannot be calculated for data with both upper and lower limits.

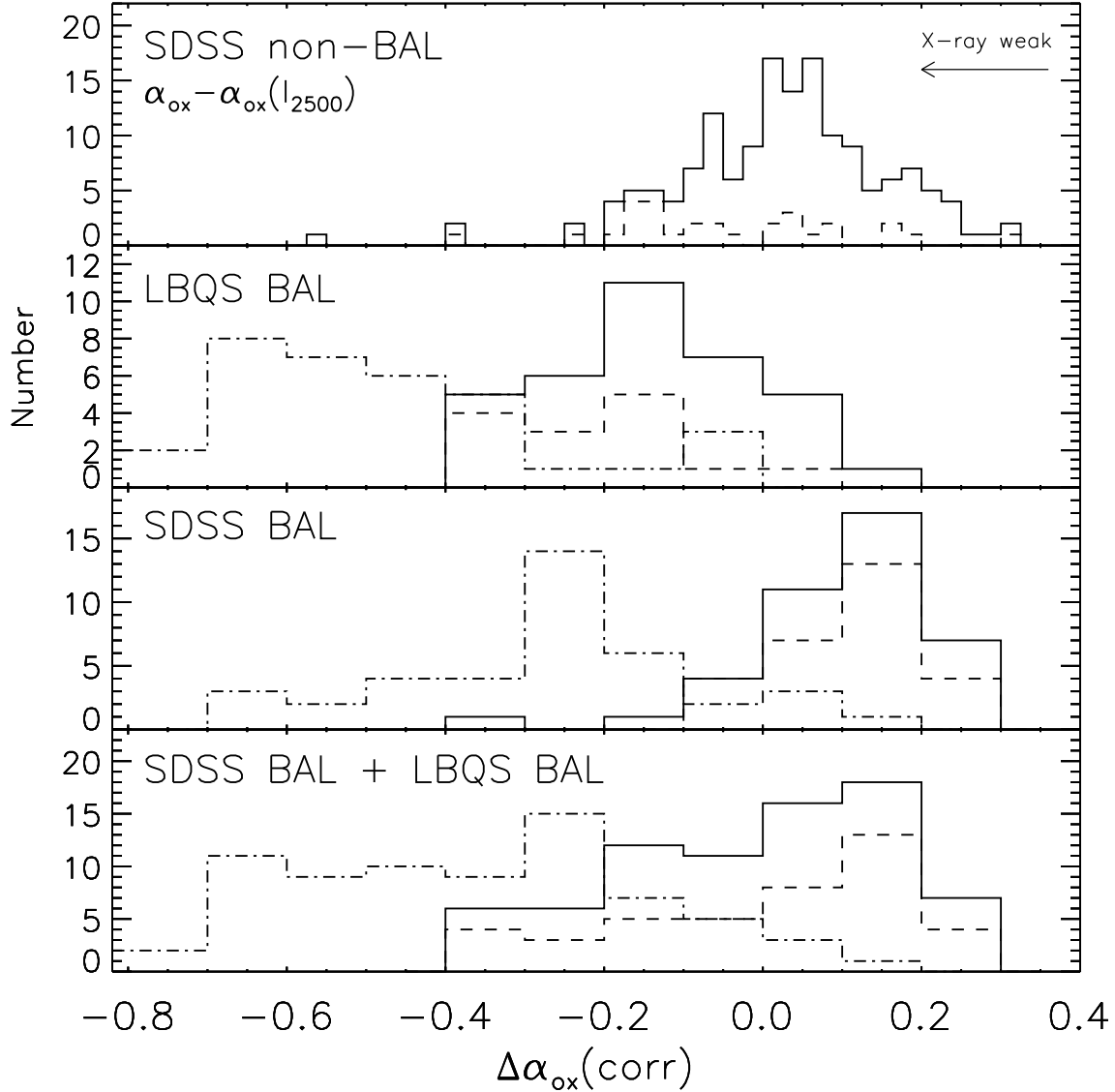


Fig. 1.— The top panel shows the distribution of observed $\Delta\alpha_{\text{ox}} = \alpha_{\text{ox}} - \alpha_{\text{ox}}(l_{2500})$ for the SDSS/*ROSAT* non-BAL sample (Strateva et al. 2005). The three lower panels show the distributions of $\Delta\alpha_{\text{ox}}(\text{corr}) = \alpha_{\text{ox}}(\text{corr}) - \alpha_{\text{ox}}(l_{2500})$ for the LBQS/*Chandra* BAL sample (G06), the SDSS/*XMM-Newton* BAL sample and the combined sample (this paper), respectively. For all four panels, solid lines indicate the full samples and dashed lines only show upper limits. Dot-dashed line in the three lower panels represents the distribution of $\Delta\alpha_{\text{ox}}$. The arrow in the top panel shows the direction of the X-ray weak objects for our convention of α_{ox} .

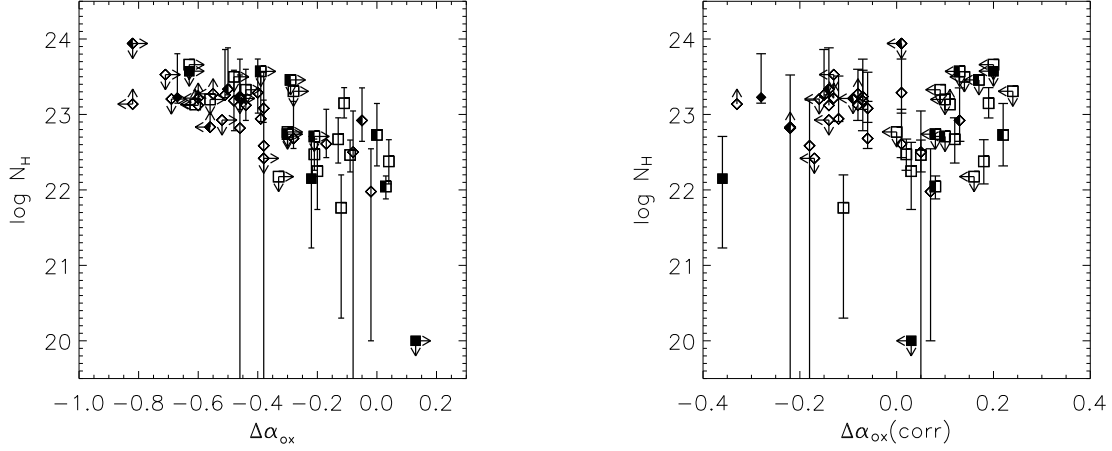


Fig. 2.— The left panel shows the N_{H} vs. $\Delta\alpha_{\text{ox}} = \alpha_{\text{ox}} - \alpha_{\text{ox}}(l_{2500})$ and the right panel shows the N_{H} vs. $\Delta\alpha_{\text{ox}}(\text{corr}) = \alpha_{\text{ox}}(\text{corr}) - \alpha_{\text{ox}}(l_{2500})$ for the detected BAL QSOs in the combined sample. SDSS BAL QSOs in our sample are shown with squares and LBQS BAL QSOs in G06’s sample are shown with diamonds. The open, filled and half-filled symbols indicate HiBALs, LoBALs and BAL QSOs of unknown type, respectively.

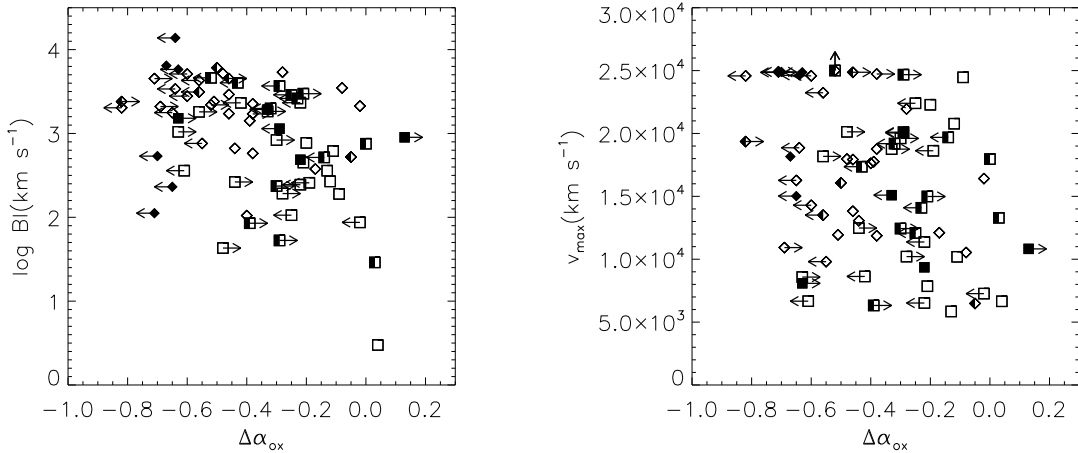


Fig. 3.— Plots of $\Delta\alpha_{\text{ox}} = \alpha_{\text{ox}} - \alpha_{\text{ox}}(l_{2500})$ vs. C IV absorption-line parameters for the combined sample : BALnicity index (BI, left panel) and maximum outflow velocity of absorption, (v_{max} , right panel). Symbols are the same as in Fig. 2.

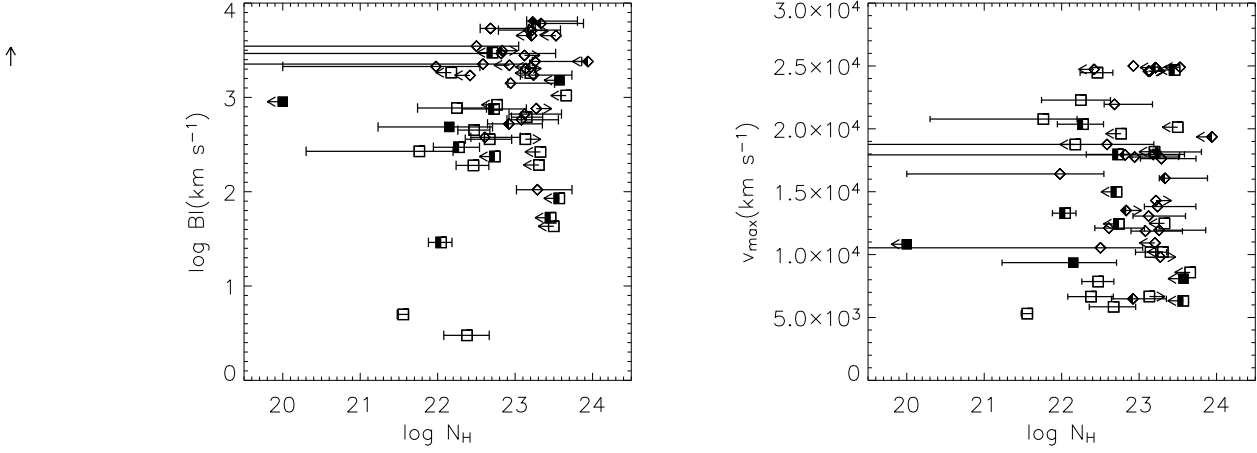


Fig. 4.— Plots of N_{H} vs. C IV absorption-line parameters for the detected BAL QSOs in the combined sample : BALnicity index(BI , left panel) and maximum outflow velocity of absorption, (v_{max} , right panel). Symbols are the same as in Fig. 2 .

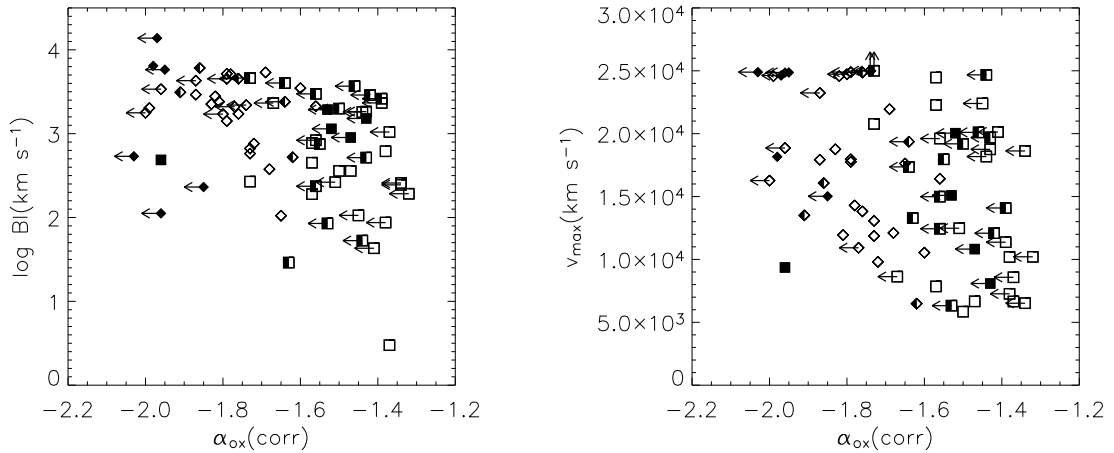


Fig. 5.— Plots of $\alpha_{\text{ox}}(\text{corr})$ vs. C IV absorption-line parameters for the combined sample : BALnicity index(BI , left panel) and maximum outflow velocity of absorption, (v_{max} , right panel). Symbols are the same as in Fig. 2 .

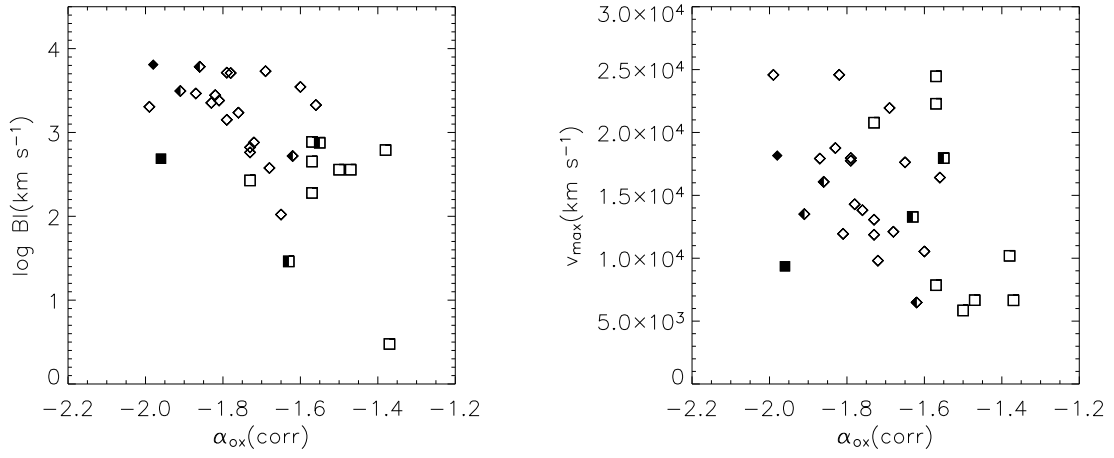


Fig. 6.— Plots of $\alpha_{\text{ox}}(\text{corr})$ vs. C IV absorption-line parameters for the BAL QSOs detected in the hard X-ray band in the combined sample : BALnicity index(BI , left panel) and maximum outflow velocity of absorption, (v_{max} , right panel). Symbols are the same as in Fig. 2 .